Int. J. Electrochem. Sci., 16 **(2021)** Article Number: 211228, doi: 10.20964/2021.12.04

International Journal of
ELECTROCHEMICAL
SCIENCE
www.electrochemsci.org

MIL-101 (Fe) modified carbon paste electrode for the efficient simultaneous detection of hydroquinone and catechol

Mengting Zhu , Ruli Xu, Xueyang Wang, Jie Liu Qianli Zhang[*], *Jie Wei*[*]

School of chemistry and life Science, Suzhou University of Science and Technology, 1 Kerui Road, Suzhou 215011, China
[*]E-mail: zqlmhb@163.com (Q. Zhang) ustsweijie@163.com (J. Wei)

Received: 14 August 2021 / *Accepted:* 27 September 2021 / *Published:* 10 November 2021

Four Fe-based metal-organic frameworks (MIL-101(Fe), MIL-53(Fe), MIL-88(Fe), and MIL-100(Fe)) were synthesized using a solvothermal method, and further characterized by X-ray diffraction, Fourier transforms infrared spectroscopy, Scanning electron microscopy, and X-ray photoelectron spectroscopy. The synthesized Fe-MOFs were used to fabricate the modified carbon paste electrodes (CPE) for simultaneous detection of hydroquinone and catechol. Among the MILs (Fe) modified CPEs, MIL-101(Fe)/CPE exhibited extraordinary electrochemical sensitivity because of MIL-101 (Fe)'s excellent conductivity. The oxidation potential separation of hydroquinone and catechol achieved 190 mV. Compared with CPE, the oxidation currents of hydroquinone and catechol at MIL-101/CPE were 10-fold higher and the reduction currents were 5-fold higher. The linear range was 2 - 90 μM for hydroquinone and 2 - 100 μM for catechol, and the detection limit was 0.58 μM and 0.62 (S/N = 3) μM for hydroquinone and catechol. Furthermore, the application of MIL-101 (Fe)/CPE has been validated in an actual river water sample with the satisfied recoveries of 90.21 - 102.36% and 91.11 - 102.19% for hydroquinone and catechol, respectively.

Keywords: Electrochemical detection, MILs (Fe), Hydroquinone and catechol, Modified carbon paste electrode, Differential pulse voltammetry

1. INTRODUCTION

Hydroquinone (HQ) and catechol (CC) are widely applied in electroplating, light stabilizers, dyes, and antioxidants. In addition, both HQ and CC are essential intermediates of the pharmaceutical industry [1,2]. However, HQ and CC are two severe environmental pollutants on account of the high toxicity and negligible degradation under natural conditions [3]. Thus, the determination of HQ and CC in ecological samples is vital to ensure the health of human beings and animals in contaminated areas. So far, electrochemical methods [4,5], high-performance liquid chromatography [6], and microfluidic

Chip [7] have been reported to detect HQ and CC. In the above-mentioned methods, electrochemical methods are particularly striking due to its' advantages of high detection sensitivity, convenient operation, and facilitating miniaturization and automation.

HQ and CC are isomers and have similar electrochemical properties. Thus, the redox of HQ and CC often overlap on a bare electrode, which leads to a challenging electrochemical experiment for the simultaneous detection of HQ and CC. To address the above issues, scientists have explored various modified electrodes including activated GO/SPCE [8], Au-Pd NF/rGO [9], AuNPs/Fe_3O_4-APTES-GO/GCE [10], NiO/MWCNT/GCE [11], $CoFe_2Se_4$/PCF/GCE [12], and poly (direct yellow 11)/MPGE [13]. The modified materials contain metal or metal oxide nanomaterial, functioned carbon, polymer, or their combination. Therefore, further seeking an advanced material with high catalytic activity is urgently needed for fabricating a sensitive electrochemical sensor for the simultaneous detection of HQ and CC.

Metal-organic frameworks (MOFs), a new type of porous solid material, have drawn considerable interest because of their merits of high specific surface area, controllable chemical components, and adjustable pore structure [14,15]. The unsaturated coordination centers in MOFs can be acted as Lewis acids which are particularly important for electrocatalysis. MOFs and their composites have been intensively investigated as electrode modification materials for the purpose of single or simultaneous determination of HQ and CC [16-20]. For instance, Li et al. [16] reported that Cu-MOF-Graphene modified glassy carbon electrode had excellent sensitivity and high selectivity for the simultaneous detection of HQ and CC, demonstrating a detection limit of 0.59 μM for HQ and 0.33 μM for CC. Deng et al. [20] confirmed that UiO-66/mesoporous carbon modified glassy carbon electrode could effectively detect HQ and CC with a peak-to-peak potential separation of 130 mV. The detection limits were 0.056 μM and 0.072 μM for HQ and CC.

The iron-based MOFs (Fe-MOFs) are of particular interest for the intriguing advantages of the fast electron transfer properties originated from Fe(III)/Fe(II) redox couple, excellent catalytic stability, iron-rich, and non-toxicity of Fe [21,22]. Nevertheless, there are few reports about Fe-MOFs modified electrodes for the simultaneous determination of HQ and CC. Herein, four typical Fe-MOFs (MIL-101, MIL-53, MIL-88, and MIL-100) are prepared using a facile conventional hydrothermal method. These Fe-MOFs modified CPEs are constructed for simultaneous determination of HQ and CC. MIL-101(Fe)/CPE demonstrates the optimum electrocatalytic performance for HQ and CC because of its superior electrical conductivity and high surface area. Scheme 1 illustrated the schematic process for simultaneous determination of HQ and CC by MIL-101(Fe)/CPE. The explored method has been applied to detect HQ and CC in the river water, and gets the satisfying recovery results, which provides impressive prospects for the application.

Scheme 1. The process of MIL-101 (Fe)'s preparation and the determination of HQ and CC by MIL-101 (Fe)/CPE.

2. EXPERIMENTAL SECTIONS

2.1. Materials and reagents

Hydroquinone (AR), catechol (AR), trimesic acid (AR), terephthalic acid (AR), and graphite powder (99.5%) were purchased from Aladdin, Shanghai. Ferric chloride hexahydrate (AR), ferric nitrate nonahydrate (AR), mineral oil (AR), potassium dihydrogen phosphate (99%), disodium hydrogen phosphate (99%), potassium ferricyanide (99%), dimethylformamide (AR) were supplied by Shanghai Lianshi chemical Co., Ltd. Phosphate buffer solution (PBS, 0.1 M) was prepared by mixing $KH_2PO_4 \cdot 2H_2O$ (0.1 M) and $Na_2HPO_4 \cdot 12H_2O$ (0.1 M), and adjusted using NaOH or HCl solution. In the electrochemical determinations, 0.1 M PBS (pH 7.0) was used unless otherwise noted.

2.2. Characterization and electrochemical determinations

XRD data were recorded on an X-ray powder diffractometer (D8-Focus, Bruker, Germany) with Cu-K radiation (λ= 0.15406 nm). Fourier transforms infrared (FTIR) spectra were obtained using a Nicolet iS50 spectrometer. Scanning electron microscopy (SEM) images were performed on a Hitachi S4800. The X-ray photoelectron spectroscopy results were obtained from an ESCALAB 250Xi XPS (Thermo Fisher, America) using Al-K radiation (h=148606 eV). C1s peak at 284.6 eV was used for the calibration.

We conduct the electrochemical determinations on an RST3100 electrochemical workstation (Suzhou, China) with a three-electrode system of a CPE (with or without modification) as the working electrode, a platinum wire as the counter electrode, and an Ag/AgCl as the reference electrode.

Electrochemical impedance spectroscopy (EIS) was carried out in 0.1 M KCl containing 5 mM $[Fe(CN)_6]^{3-/4-}$ in the frequency range of 1~10^5 Hz. The potential window of cyclic voltammetry (CV) and differential pulse voltammetry (DPV) was -0.2 - 0.8 V.

2.3. Preparation of MILs (Fe)

According to the reported references [15, 22-24], MILs (Fe) were prepared using the hydrothermal reaction of terephthalic acid or trimesic acid with Fe^{3+} by controlling different molar ratios, solvent, temperature, and time. The synthesis procedure of MIL-101(Fe) [15] was as follows: 5 mmol $FeCl_3 \cdot 6H_2O$ and 2.5 mmol terephthalic acids were firstly mixed in 30 mL DMF, after being sonicated for 30 min, the mixture solution was sealed into a Teflon-lined stainless steel autoclave, and then heated at 110℃ for 24 h. Orange mud was obtained after centrifugation. The mud was washed using DMF, EtOH, and H_2O for 3 times, and then vacuum dried at 60℃. MIL-53(Fe) [22] was prepared following a similar procedure except that 1 mmol $FeCl_3 \cdot 6H_2O$ and 1 mmol terephthalic acid were mixed in 6 mL DMF and heated at 150℃ for 3 h. MIL-88(Fe) [24] followed a comparable production procedure with the above two except that the mixture of 1 mmol $FeCl_3 \cdot 6H_2O$, 1 mmol terephthalic acid, 0.8 mmol NaOH, and 5 mL DMF was heated at 100℃ for 16 h.

For the preparation of MIL-100 (Fe) [24], 2 mmol trimesic acid was reacted with 4 mmol $Fe(NO_3)_3 \cdot 9H_2O$ in the mixture solution of 4 mmol HF, 1.2 mmol nitric acid, and 554 mmol H_2O. The reactant mixture was loaded in a Teflon autoclave and heated at 150℃ for 12 h. MIL-100(Fe) was washed using DMF, EtOH, and H_2O for 3 times, and vacuum dried at 60℃.

2.4. Fabrication of the MILs (Fe) modified CPE

MILs (Fe) were mixed sufficiently with graphite powder and methyl silicone oil (weight ration 32:1:17) in an agate mortar. And then, we tightly filled the paste into a CPE mold (3.0 mm in diameter) and smoothed the electrode surface with weighing papers. For comparison, the CPE was prepared by a similar procedure without the addition of MILs (Fe).

3. RESULTS AND DISCUSSION

3.1. The characterization of MILs (Fe)

Fig. 1A displays the XRD patterns of MIL-53(Fe), MIL-88(Fe), MIL-100(Fe), and MIL-101(Fe). Characteristic diffraction peaks are found in MILs (Fe), indicated the obtaining of well-crystallized MOF structures. The peaks near 10° result from the various topologies and crystal structures of Fe-MOFs [22]. In addition, other diffraction peaks are consistent with those reported in the literature [15,22], indicating the successful synthesis of Fe-MOFs. Fig. 1B shows the FT-IR spectra of MILs (Fe). As can be seen, MIL-53 (Fe), MIL-88 (Fe), and MIL-101 (Fe) have similar IR spectra due to the use of the same ligand terephthalic acid. The characteristic peak at 1662 cm^{-1} is counterpart to the C=O stretching vibration

peak of the carboxyl group. The peaks at 1592 cm^{-1} and 1392 cm^{-1} are related to the asymmetric and symmetric vibrations of the C=O group, respectively. The peak at 750 cm^{-1} is the result of C-H bending vibration in the benzene ring. While the peak at 549 cm^{-1} is attributed to the Fe-O stretching vibration [25]. However, MIL-100 (Fe)'s corresponding peaks shifted to 1626, 1577, 1382, 712, 487 cm^{-1}, respectively. The shifts may result from the different use of trimesic acid in MIL-100 (Fe).

Fig. 1 also shows the SEM images of MILs (Fe). MIL-101 (Fe) consists of smooth surface crystals of 0.2 - 0.4 μm (Fig. 1C). MIL-53 (Fe) morphology is a crystalline cubic structure with an average size of 10 μm (Fig. 1D). MIL-88 (Fe) is observed in the shape of spindle with a size of 1.4×0.3 μm in length and width (Fig.1E), which resembles the previous studies [26]. Besides, MIL-100(Fe) shows an irregular crystal morphology with a diameter from 1 μm to 2 μm (Fig. 1F). As shown from the above results, MIL-101 (Fe) has the smallest particle size, indicating that it has the largest specific surface area and large amount of electrochemical active sites, and is expected to have the best electrocatalytic activity for the redox of HQ and CC.

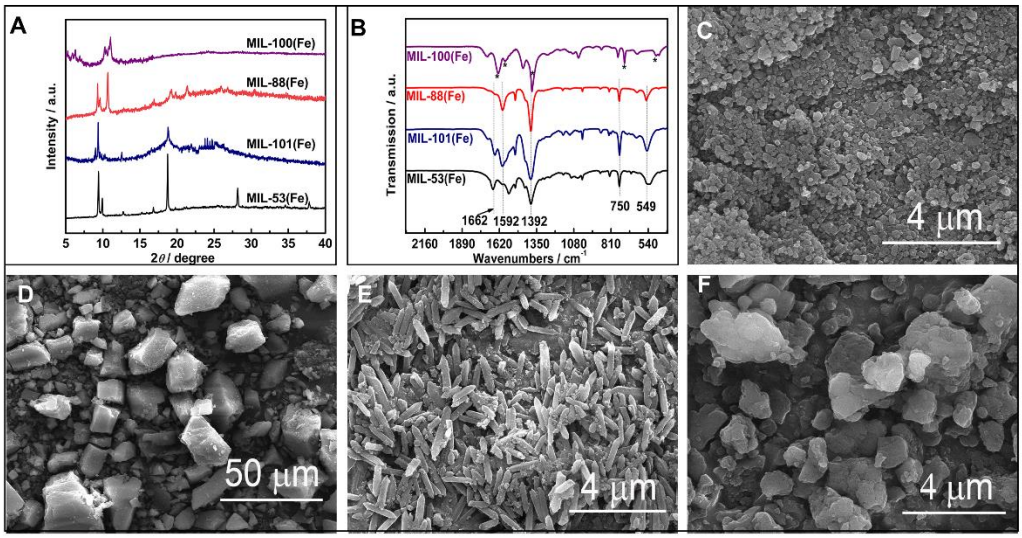

Figure 1. (A) XRD of MILs (Fe), (B) FT-IR spectra of MILs (Fe), and SEM image of MIL-101(Fe) (C), MIL-53(Fe) (D), MIL-88(Fe) (E), MIL-100(Fe) (F)

The chemical composition and valence states of MIL-101 (Fe) were analyzed by XPS spectroscopy. XPS full spectrum of MIL-101 (Fe) (Fig. 2A) shows the presence of C, O, and Fe. Three peaks at 284.77 eV, 285.26 eV, and 288.75 eV of C 1s spectrum (Fig. 2B) are attributed to C-H/C-C, C-O, and O-C=O, respectively. The peaks at 531.10 eV, 531.94 eV, and 532.95 eV in O 1s spectrum (Fig. 2C) are ascribed to Fe-O, -COOH, and -OH, respectively. In Figure 2D, two peaks at 711.96 eV and 725.49 eV in Fe 2p spectrum are from Fe $2p^{1/2}$ and Fe $2p^{3/2}$ [27].

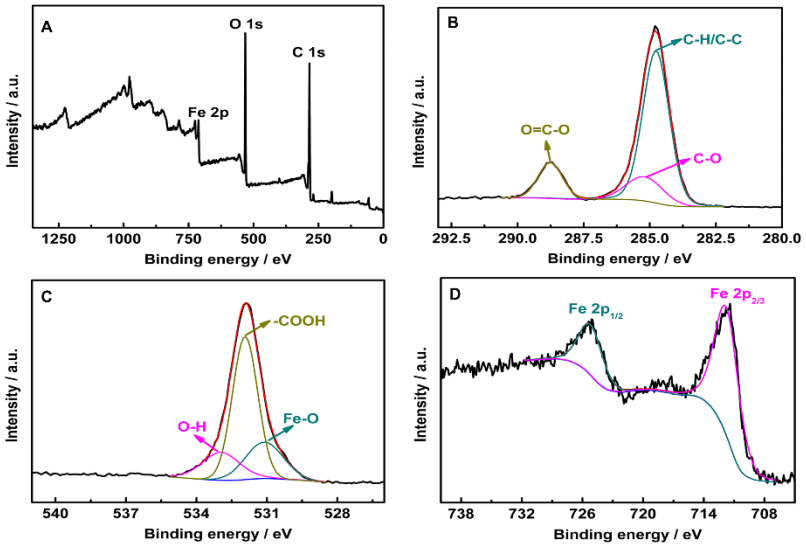

Figure 2. XPS survey (A) and high-resolution XPS of C 1s (B), O 1s (C) and Fe 2p (D) spectra of MIL-101 (Fe).

3.2. Electrocatalytic of HQ and CC at MILs (Fe)/CPE.

Fig. 3A and Fig. 3B depict cyclic voltammograms of different modified electrodes in 80 μM HQ and CC with a buffer solution of 0.1 M PBS (pH 7.0) at 50 mV/s. There are two distinct reduction peaks at 0.05 and 0.16 V corresponding to the reduction of HQ and CC at the CPE. However, the oxidation of HQ and CC cannot be distinguished, and only a broad peak at 0.24 V is observed. The oxidation of HQ and CC on MIL-88 (Fe)/CPE and MIL-53 (Fe)/CPE cannot be distinguished and exhibits as a broad oxidation peak too. The oxidation performance of HQ and CC progresses slightly on MIL-100 (Fe)/CPE, showing two weak oxidation peaks at 0.1 and 0.24 V. The above experimental results indicate that MIL-88 (Fe)/CPE, MIL-53 (Fe)/CPE, and MIL-100 (Fe)/CPE had no significant catalytic effect on the redox of HQ and CC. While the redox of HQ and CC is greatly enhanced at MIL-101 (Fe)/CPE, and two pairs redox peaks in Fig. 1A clearly demonstrate the redox of HQ and CC. As opposed to CPE, the oxidation currents of HQ and CC were approximately 10-fold higher. The increased detection sensitivity was superior to N-doped carbon nanotube frameworks modified electrode [28], indicating easier electron transfer at the MIL-101 (Fe)/CPE interface.

In order to understand the charge transport and conductivity of the electrode surfaces, electrochemical impedance spectroscopy (EIS) of CPE, MIL-53(Fe)/CPE, MIL-88(Fe)/CPE, MIL-100(Fe)/CPE, and MIL-101(Fe)/CPE was carried out in 0.1 M KCl containing 0.1 mM $[Fe(CN)_6]^{3-/4-}$. Fig. 3C shows the Nyquist plots of the above electrodes. The semicircle of the high-frequency region is related to the charge transfer resistance (R_{ct}) of the surface between electrode and electrolyte solution. As shown in Fig. 3C, the Rct of MIL-53 (Fe)/CPE, MIL-88 (Fe)/CPE, CPE, MIL-100 (Fe)/CPE, and MIL-101 (Fe)/CPE decreases sequentially, indicating that the conductivity of the above electrodes increases successively. MIL-101 (Fe)/CPE shows the lowest charge transfer resistance and is favorable for HQ and CC simultaneous determination. The results agree with those of the cyclic voltammetry.

We investigated the response of modified CPEs prepared with different MIL-101 (Fe) percentage in 80 μM HQ and CC solutions. As shown in Fig. 3D, the oxidation peak currents of HQ and CC initially rise with increasing of MIL-101 (Fe) content, and the oxidation peak currents of HQ and CC reach the maximum when the ratio of MIL-101 (Fe) is 1%. The oxidation peak currents of HQ and CC decrease slightly if the content of MIL-101 (Fe) increases further. Therefore, MIL-101 (Fe) ratio is chosen to be 1% in the subsequent electrochemical experiments.

Electrochemical experiments were performed at different pH values to investigate the effect of pH for simultaneous determination of HQ and CC using MIL-101 (Fe)/CPE. Fig. 3E shows the plots of pH versus the oxidation currents of HQ and CC at 50 mV/s. For HQ, the oxidation peak current increases with increasing pH in the range of 6.2-7.4 and decreases when pH is higher than 7.4. The oxidation current of CC shows a similar trend in the range of pH values investigated, while the maximum peak oxidation current is found at pH 7.0. Considering that the peak oxidation currents of HQ at pH 7.0 (51 μA) and 7.4 (53 μA) are closer, pH 7.0 is chosen as the most suitable pH value for simultaneous detecting HQ and CC. Fig. 3F shows the relationship between pH and oxidation potential (Epa) of HQ and CC. When the pH value increase from 6.2 to 7.8, a linear decrease is displayed for Epa of both HQ and CC, and the linear equations were Ep(mV) = 0.565-0.0655pH (R^2=0.995) and Ep(mV) = 0.642-0.0615pH (R^2= 0.993) for HQ and CC. The slope is very close to the typical value of the Nernst equation (-0.0592), indicating that the protons number involved in the oxidation process of HQ and CC is equal to the involved electron number. Epa of HQ is 190 mV lower than that of CC at the same pH. The potential separation of HQ and CC is 90 mV larger than that on Ce-MOF/carbon nanotube composite modified GC electrode [18], indicating the effective performance for simultaneous determination of HQ and CC at MIL-101 (Fe)/CPE.

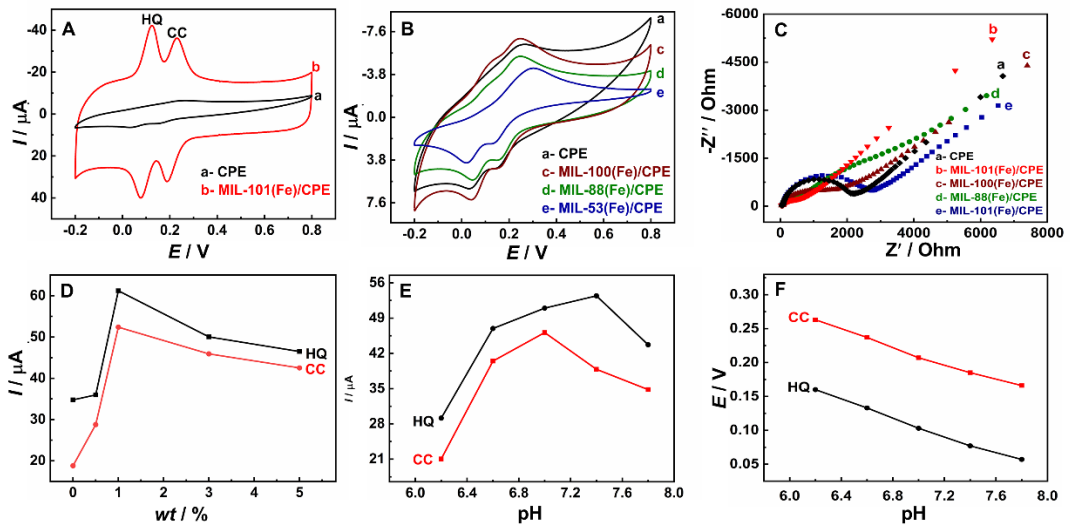

Figure 3. (A) The CVs of CPE and MIL-101 (Fe)/CPE, (B) The CVs of CPE, MIL-53 (Fe)/CPE, MIL-88 (Fe)/CPE, and MIL-100 (Fe)/CPE. (C) Electrochemical impedance spectra (Nyquist plots) of CPE, MIL-101 (Fe)/CPE, MIL-53 (Fe)/CPE, MIL-88 (Fe)/CPE, and MIL-100 (Fe)/CPE in 0.1 M KCl containing 0.1 mM $[Fe(CN)_6]^{3-/4-}$, (D) The effect of MIL-101(Fe) ratio, (E) The effect of pH on Ipa of HQ and CC, (F) The effect of pH on Epa of HQ and CC. The concentration of HQ and CC in A, B, D, E, and F: 80 μM, Buffer: 0.1 M PBS (pH 7.0), Scan rate: 50 mV/s.

Fig. 4 displays the cyclic voltammograms of MIL-101(Fe)/CPE at different sweep rates in 80 μM HQ (Fig. 4A) and 80 μM CC (Fig. 4C). The redox peak currents of HQ and CC increase with increasing the sweep rate in the range of 10-350 mV/s. The shape of the cyclic voltammograms remains even at high sweep rates, which indicates the superior capability of MIL-101(Fe)/CPE. When the sweep rate increases, the oxidation peak potentials of HQ and CC shift to a more positive direction, while the reduction peak potentials of HQ and CC shift to a more negative direction, resulted from the increased electrode polarization. The linear relationship between the peak currents (Ipa and Ipc) and the square root of the sweep rate is shown in Figures 4B and 4D. The corresponding regression equation for HQ is Ipa (μA) = -18.15 + 4.83 $v^{1/2}$ (mV/s) (R^2=0.991) and Ipc (μA) = 23.08 - 6.28 $v^{1/2}$ (mV/s) (R^2=0.992), and the regression equation for CC is Ipa (μA) = -21.89 + 5.99 $v^{1/2}$ (mV/s) (R^2=0.996) and Ipc (μA) = 25.28 - 6.56 $v^{1/2}$ (mV/s) (R^2=0.994), showing that the simultaneous determination of HQ and CC is controlled by a diffusion process.

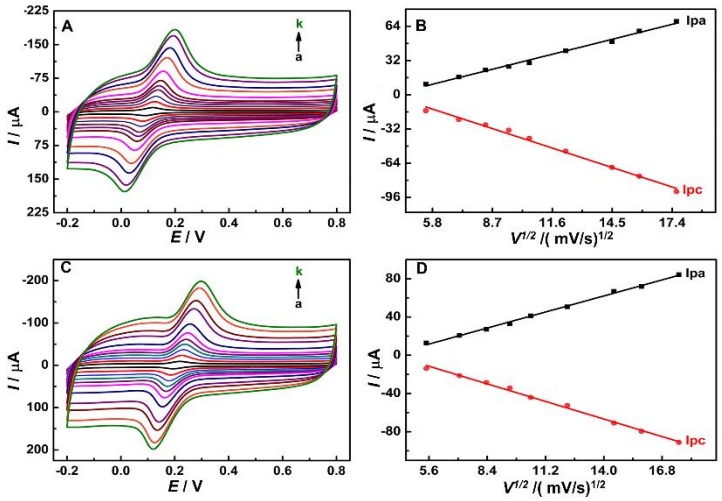

Figure 4. CV curves of the MIL-101(Fe)/CPE in PBS (pH 7.0) containing 80 μM HQ (A) and CC (C) at varied scan rate (10 - 350 mV/s); The polts of oxidation peak current (Ipa) and reduction peak current (Ipc) of HQ (B) and CC (D) versus scan rates at square root.

3.3. Simultaneous determination of HQ and CC

Fig.5A and Fig.5B display DPV of HQ and CC at different concentrations. The oxidation peak currents of HQ and CC linearly increase when the concentration of HQ or CC increases in a single-analyte solution. MIL-101(Fe)/CPE offers different detection sensitivity in low and high concentrations. In a low concentration solution, MIL-101(Fe)/CPE possesses sufficient active sites, which leads to higher detection sensitivity. However, the active sites might be saturated in a concentrated analyte, resulting in a slightly decreased detection sensitivity. Specifically, the regression equations of HQ are Ipa (μA) = 0.517 C（μM） + 0.981 (R^2 = 0.993, 2 - 20 μM) and Ipa (μA) = 0.245 C（μM） + 4.08 (R^2 = 0.987, 20 - 90 μM). The detection limit of HQ is 0.58 μM (S/N = 3). Similarly, the linear range of CC is 2 - 50 μM and 50 - 100 μM with the regression equations of Ipa (μA) = 0.412 C（μM） + 2.189 (R^2

= 0.994, 2 - 50 μM) and Ipa (μA) = 0.225 C（μM） + 11.15 (R^2 = 0.989, 50 - 100 μM). The detection limit of CC is 0.62 μM (S/N = 3). In the regression equation, C represents the concentration of HQ or CC.

DPV of the mixture solution of HQ and CC are recorded to investigate the effective of MIL-101(Fe)/CPE for simultaneous detection of HQ and CC. Two well-distinguished oxidation peaks are obtained at 8 mV and 198 mV for HQ and CC. Fig. 5C exhibits the DPV response of MIL-101(Fe)/CPE in various concentrations of HQ solution (5 - 110 μM) containing 30 μM CC. The corresponding regression equations are Ipa (μA) = 0.314 C（μM） + 0.241 (R^2 = 0.998, 5-35 μM) and Ipa (μA) = 0.143 C（μM） + 5.57 (R^2 = 0.994, 35-110 μM). Furthermore, DPV responses in the mixture contained 15 μM HQ and different concentrations of CC (5 - 110 μM) are recorded in Fig.5D. The corresponding regression equations are Ipa (μA) = 0.187 C（μM） - 0.222 (R^2 = 0.998, 5 - 60 μM) and Ipa (μA) = 0.120 C（μM） + 3.19 (R^2 = 0.997, 60 - 110 μM).

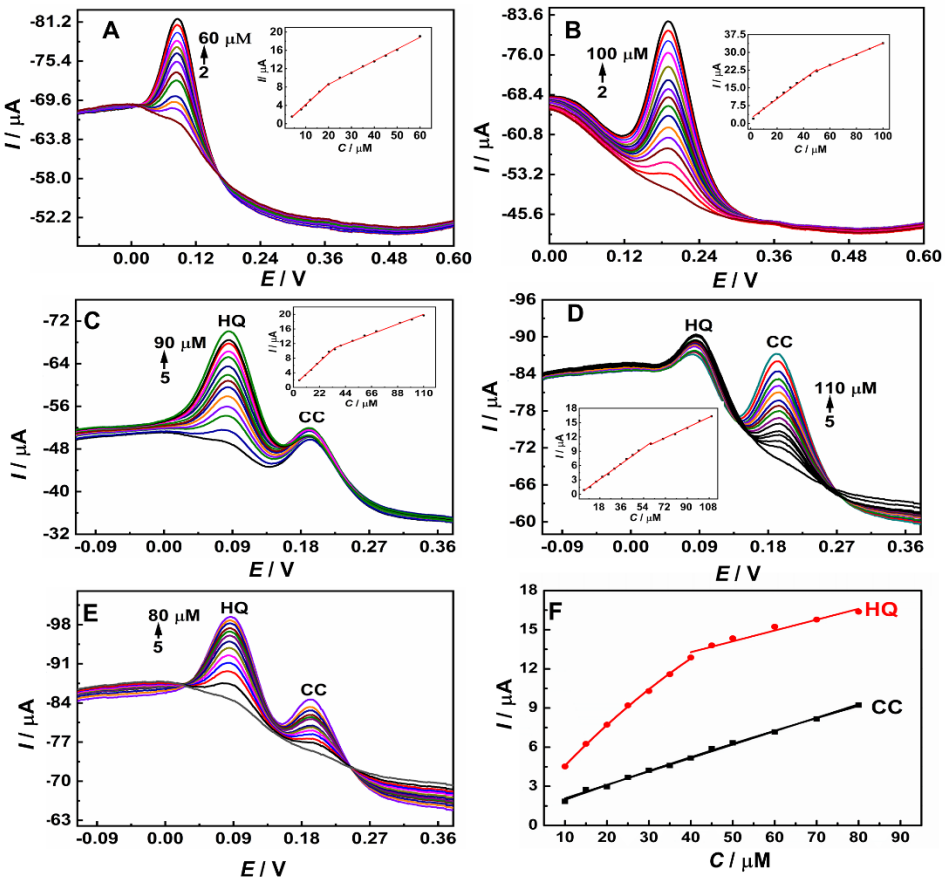

Figure 5. DPV of the MIL-101(Fe)/CPE in PBS (0.1 M, pH 7.0) containing HQ (2 - 90 μM) (A), CC（2 - 100 μM）(B), HQ (5 - 90 μM) and 30 μM CC (C), 15 μM HQ and CC (5 - 110 μM) (D), and the mixture of various concentrations of HQ and CC (5 - 80 μM) (E), and the corresponding calibration curves of HQ and CC in E (F). Insert: the corresponding linear relationships between the oxidation peak currents and concentrations of HQ and CC in A, B, C, and D.

DPV of MIL-101(Fe)/CPE is also conducted in a mixture solution of HQ and CC concentration varied simultaneously (Fig.5E). The good linear relationship can be confirmed by the following regression equations: Ipa (μA) = 0.263 C（μM） + 2.28 (R^2 = 0.993, 10 - 45 μM) and Ipa (μA) = 0.0736 C（μM） + 10.69 (R^2 = 0.994, 45 - 80 μM) for HQ, and Ipa (μA) = 0.103 C（μM） + 1.05 (R^2 = 0.996, 10 - 80 μM) for CC. Compared with those MOFs-based modified electrodes in previous reports, the detection performance of MIL-101(Fe)/CPE is comparable concerning the linear range or detection limit (Table 1). Moreover, using MIL-101(Fe) as the only electrode modification material can result in the electrode preparation process simple and effective.

Table 1. Comparison of the performances of MOFs-based modified electrodes for the simultaneous detection of HQ and CC.

Electrode	Linear range (μM)		LOD (μM)		Ref
	HQ	CC	HQ	CC	
UiO-66/MC/GCE	0.5 - 100	0.4 - 100	0.056	0.072	[20]
MIL-101(Cr)/rGO/CPE	10 - 1400	4 - 1000	4.0	0.66	[17]
$Cu_3(btc)_2$/CS/ERGO/GCE	5 - 200	5 - 200	0.44	0.43	[29]
Cu-MOF-199-ERGO/GCE	0.1 - 476	0.1 - 476	0.1	0.1	[30]
Cu-MOF-GN/GCE	1 - 1000	1 - 1000	0.59	0.33	[31]
HKUST-1/CPE		0.8 - 32		0.1	[32]
MIL-101(Fe)/CPE	2 - 90	2 - 100	0.58	0.62	This work

MC：mesoporous carbon；ERGO, rGO：reduced graphite oxide；CS：chitosan；

3.4. Stability and selectivity determinations

Five duplicated MIL-101(Fe)/CPE was conducted to detected 80 μM HQ or CC to investigate the reproducibility. The relative standard deviations of oxidation peak currents for HQ and CC are 3.16% and 3.22%, which is comparable with the stability of activated graphene oxide modified electrode [33].

Furthermore, the stability of MIL-101(Fe)/CPE is investigated by the detection performance of freshly prepared electrode and the modified electrode after 3, 5, 10 days. After five days, the oxidation peak currents of HQ and CC keep 97% and 93% of the initial current, and the oxidation peak currents remain 89% and 86% after ten days. Hence, MIL-101(Fe)/CPE exhibits a high reproducibility and a satisfied long-term stability for the simultaneous detection of HQ and CC.

The selectivity of MIL-101(Fe)/CPE is evaluated using the DPV responses of 80 μM HQ or CC in the presence of different interfering substances. Common inorganic ions such as CO_3^{2-}, SO_4^{2-}, Cl^-, NO_3^-, Na^+, K^+, Zn^{2+}, Cu^{2+}, Mg^{2+} do not interfere the detection of HQ and CC in 100-fold excess. Some organic or biological molecules, such as glucose, uric acid, ascorbic acid, do not cause a noticeable change for the oxidation peak current of HQ and CC in 10-fold excess. The above results testified that MIL-101(Fe)/CPE possesses prominent selectivity and anti-interference ability to detect HQ and CC in an actual sample.

MIL-101(Fe)/CPE is used to detect HQ and CC in river water samples (from Suzhou, China) for evaluating its applicability. Neither HQ nor CC has been detected in the real sample. The recoveries of HQ and CC are obtained using spiking the HQ and CC. The recoveries of HQ and CC are 90.21 - 102.36% and 91.11 - 102.19% (Table 2), indicating that the detection of HQ and CC with MIL-101(Fe)/CPE is reliable.

Table 2. Detection of HQ and CC in river water

Sample	Add (μM)		Found (μM)		Recovery（%）	
	HQ	CC	HQ	CC	HQ	CC
1	40	40	39.02	39.37	97.54	98.43
			36.08	38.89	90.21	97.22
			36.99	39.36	92.47	98.39
2	60	60	59.49	58.71	99.15	97.85
			61.42	61.31	102.36	102.19
			59.70	58.77	99.50	97.95
3	80	80	75.58	76.70	94.48	95.88
			74.85	72.89	93.56	91.11
			75.51	80.54	94.39	100.68

4. CONCLUSION

In conclusion, MIL-101(Fe)/CPE, a novel electrochemical sensor, is prepared for the simultaneous detection of HQ and CC. Under the optimized conditions, the peak-to-peak potential separation between HQ and CC is 190 mV, higher than the values reported in most of the literature. In addition, MIL-101(Fe)/CPE exhibited good reproducibility and stability in simultaneous detecting HQ and CC. MIL-101(Fe)/CPE broaden MOFs' application in electrochemical sensors.

FUNDING
This work is supported by the NSFC (No. 20905055, 511782, and 21702143) and the open projects from College of Chemistry and Molecular Engineering of Qingdao University of Science and Technology (QUSTHX201906).

References

1. Y. Wang, X. Chen, D. Huang, T. Jin, *Int. J. Electrochem.* Sc., 15(2020)6620.
2. T. Chen, S. Palanisamy, S. Chen, V. Velusamy, Y. Liu, T. Tseng, M. Yu, S. Lee, W. Chang, X. Liu, *Int. J. Electrochem. Sc.*, 12(2017)8021.
3. S. Ramaraj, S. Mani, S. Chen, T. Kokulnathan, B. Lou, M. A. Ali, A. A. Hatamleh, F. M. A. Al-Hemaid, *J. Colloid Interf. Sci.*, 514(2018)59.
4. Ç. C. Koçak, S. Koçak, *Electroanalysis*, 32(2019)358.
5. S. Koçak, *Electroanal.*, 33(2021)375.
6. X. Luo, H. Zheng, Z. Zhang, M. Wang, B. Yang, L. Huang, M. Wang, *Microchem. J.*, 137(2018)148.

7. J. Qi, B. Li, X. Wang, L. Fu, L. Luo, L. Chen, *Anal. Chem.*, 90(2018)11827.
8. M. Velmurugan, N. Karikalan, S. Chen, Y. Cheng, C. Karuppiah, *J. Colloid Interf. Sci.*, 500(2017)54.
9. Y. Chen, X. Liu, S. Zhang, L. Yang, M. Liu, Y. Zhang, S. Yao, *Electrochim. Acta*, 231(2017)677.
10. S. Erogul, S. Z. Bas, M. Ozmen, S. Yildiz, *Electrochim. Acta*, 186(2015)302.
11. L. A. Goulart, L. H. Mascaro, *Electrochim. Acta*, 196(2016)48.
12. D. Yin, J. Liu, X. Bo, L. Guo, *Anal. Chim. Acta*, 1093(2020)35.
13. K. Chetankumar, B. E. Kumara Swamy, S. C. Sharma, *Microchem. J.*, 156(2020)104979.
14. G. Fang, J. Zhou, C. Liang, A. Pan, C. Zhang, Y. Tang, X. Tan, J. Liu, S. Liang, *Nano Energy*, 26(2016)57.
15. H. Hu, H. Zhang, Y. Chen, Y. Chen, L. Zhuang, H. Ou, *Chem. Eng. J.*, 368(2019)273.
16. J. Li, J. Xia, F. Zhang, Z. Wang, Q. Liu, *Talanta*, 181(2018)80.
17. H. Wang, Q. Hu, Y. Meng, Z. Jin, Z. Fang, Q. Fu, W. Gao, L. Xu, Y. Song, F. Lu, *J. Hazard. Mater.*, 353(2018)151.
18. H. Huang, Y. Chen, Z. Chen, J. Chen, Y. Hu, J. Zhu, *J. Hazard. Mater.*, 416(2021)125895.
19. T. Zhang, J. Wei, X. Sun, X. Zhao, H. Tang, H. Yan, F. Zhang, *Inorg. Chem.*, 59(2020)8827.
20. M. Deng, S. Lin, X. Bo, L. Guo, *Talanta*, 174(2017)527.
21. Y. Gong, B. Yang, H. Zhang, X. Zhao, *J. Mater. Chem. A*, 6(2018)23703.
22. D. Yu, M. Wu, Q. Hu, L. Wang, C. Lv, L. Zhang, *J. Hazard. Mater.*, 367(2019)456.
23. N. A. Ramsahye, T. K. Trung, L. Scott, F. Nouar, T. Devic, P. Horcajada, E. Magnier, O. David, C. Serre, P. Trens, *Chem. Mater.*, 25(2013)479.
24. E. Soubeyrand-Lenoir, C. Vagner, J. W. Yoon, P. Bazin, F. Ragon, Y. K. Hwang, C. Serre, J. Chang, P. L. Llewellyn, *J. Am. Chem. Soc.*, 134(2012)10174.
25. D. Yan, H. Hu, N. Gao, J. Ye, H. Ou, *Appl. Surf. Sci.*, 498(2019)143836.
26. N. M. Mahmoodi, J. Abdi, M. Taghizadeh, A. Taghizadeh, B. Hayati, A. A. Shekarchi, M. Vossoughi, *J. Environ. Manage.*, 233(2019)660.
27. B. Liu, Y. Wu, X. Han, J. Lv, J. Zhang, H. Shi, *J. Mater. Sci.: Mater. El.*, 29(2018)17591.
28. X. Zheng, Y. Hu, H. Li, B. Han, R. Lin, B. Huang, *J. Electroanal. Chem.*, 861(2020)113968.
29. Y. Yang, Q. Wang, W. Qiu, H. Guo, F. Gao, *J. Phys. Chem C*, 120(2016)9794.
30. Q. Chen, X. Li, X. Min, D. Cheng, J. Zhou, Y. Li, Z. Xie, P. Liu, W. Cai, C. Zhang, *J. Electroanal. Chem.*, 789(2017)114.
31. D. Brondani, E. Zapp, R. Da Silva Heying, B. de Souza, I. Cruz Vieira, *Electroanalysis*, 29(2017) 2810.
32. Y. Ai, N. Gao, Q. Wang, F. Gao, D. B. Hibbert, C. Zhao, *J. Electroanal. Chem.,* 872(2020)114161.
33. M. Velmurugan, N. Karikalan, S. Chen, Y. Cheng, C. Karuppiah, *J. Colloid Interf. Sci.,* 500(2017) 54.